crystals

MDPI

Article

Effect of TiO_2 Content on the Corrosion and Thermal Resistance of Plasma-Sprayed Al_2O_3-TiO_2 Coatings

Viktorija Grigaitienė [1,*], Liutauras Marcinauskas [1], Airingas Šuopys [1], Romualdas Kėželis [1] and Egidijus Griškonis [2]

[1] Plasma Processing Laboratory, Lithuanian Energy Institute, Breslaujos Str. 3, LT-44403 Kaunas, Lithuania; liutauras.marcinauskas@lei.lt (L.M.); airingas.suopys@lei.lt (A.Š.); romualdas.kezelis@lei.lt (R.K.)

[2] Faculty of Chemical Technology, Kaunas University of Technology, LT-44249 Kaunas, Lithuania; egidijus.griskonis@ktu.lt

[*] Correspondence: viktorija.grigaitiene@lei.lt

Abstract: Modern industrial systems and biomass-fired furnaces require surface treatments that can withstand aggressive chemical, thermal, and corrosive environments. This study investigates the corrosion and thermal resistance of plasma-sprayed Al_2O_3-TiO_2 coatings produced using a DC air–hydrogen plasma spray process. Coatings of compositions of Al_2O_3, Al_2O_3-3 wt.% TiO_2, Al_2O_3-13 wt.% TiO_2, and Al_2O_3-40 wt.% TiO_2 were deposited on steel substrates with a Ni/Cr bond layer by plasma spraying. The coatings were characterized by scanning electron microscopy (SEM), energy-dispersive X-ray spectroscopy (EDS), and X-ray diffraction (XRD) to evaluate their morphology, elemental composition, and crystalline phases. Electrochemical tests were performed in a naturally aerated 0.5 mol/L NaCl solution and cyclic thermal–chemical exposure tests (500 °C using 35% KCl) to assess their corrosion kinetics and thermal stability. The results indicate that pure Al_2O_3 and low TiO_2 (3 wt.%) coatings exhibit fine barrier properties, while coatings with a higher TiO_2 content develop additional phases (e.g., Ti_3O_5, Al_2TiO_5) that improve thermal resistance but reduce chemical durability.

Keywords: Al_2O_3-TiO_2 coatings; plasma spraying; DC plasma torch; coating morphology; corrosive resistance

check for updates

Academic Editors: George D. Verros and Vladislav V. Kharton

Received: 14 March 2025
Revised: 15 April 2025
Accepted: 30 April 2025
Published: 3 May 2025

Citation: Grigaitienė, V.; Marcinauskas, L.; Šuopys, A.; Kėželis, R.; Griškonis, E. Effect of TiO_2 Content on the Corrosion and Thermal Resistance of Plasma-Sprayed Al_2O_3-TiO_2 Coatings. *Crystals* **2025**, *15*, 439. https://doi.org/10.3390/cryst15050439

1. Introduction

The need for functional materials is continuously increasing as modern systems and their components must withstand harsh chemical, thermal, and corrosive environments. In many cases, surface treatment to change their properties is essential to ensure enhanced performance, longevity, and quality. Protective ceramic coatings, especially those deposited by plasma spraying, offer a promising alternative to traditional organic or polymer-based coatings for surface protection. Metal oxide ceramics such as alumina, zirconia, titania, yttria, and their compounds are widely used because of their high melting points, chemical inertness, and excellent thermal stability [1].

Plasma spray technology is widely applicable due to its low cost, flexibility, easy process control, and high deposition rates that allow for coverage of large and complex surfaces of substrates. Plasma jets, operating at temperatures between 2000 and 14,000 K and reaching velocities from 100 to 2500 m/s, enable effective melting and deposition of a wide variety of materials [1–8]. The parameters of the plasma spray process, such as the power of the plasma torch, the gas flow rate, and the gas type, can be precisely controlled to achieve the required properties. A direct current (DC) plasma torch developed at the Lithuanian Energy Institute is made of a hot-button-type hafnium cathode and a high-purity copper anode is used to generate a stable electric arc under atmospheric conditions [4,5].

In biomass-fired furnaces, straw combustion produces compounds that contain potassium, sodium, and chlorine. Chlorine is released as HCl and Cl_2, which react with fire grate surfaces and cause severe active oxidation corrosion, drastically reducing the service life of metal grates. Protecting steel surfaces with ceramic coatings can extend the lifespan of steel elements and reduce exploitation and maintenance costs. Although numerous studies have examined coatings produced using argon or argon–hydrogen plasmas [1,8,9], research on coatings formed using an air–hydrogen plasma in atmospheric plasma spraying (APS) remains limited. Moreover, an understanding of the plasma spray process parameters, which influence the crystal structure and phase composition, is therefore essential. Al_2O_3-TiO_2 ceramic coatings attract considerable attention because they combine the high hardness and chemical inertness of alumina with the enhanced fracture toughness and binding properties provided by titania. Early investigations by different authors demonstrated that increasing the TiO_2 content can improve thermal control and corrosion resistance; however, an overlarge quantity of titania can reduce hardness due to changes in phase composition [1,10]. W. Lan et al. [10] found that the corrosion current densities of the Al_2O_3 and Al_2O_3-13 wt,% TiO_2 coatings were 0.36 $\mu A/cm^2$ and 0.095 $\mu A/cm^2$, respectively. The improved corrosion resistance was attributed to the reduction in the porosity and enhanced density of the coatings. High cooling rates during the plasma spray process often result in the formation of metastable alumina phases (e.g., γ-Al_2O_3) rather than thermodynamically stable α-Al_2O_3, while titania can crystallize as anatase or rutile. In specific compositions, intermetallic compounds such as Ti_3O_5 and Al_2TiO_5 can form, affecting the thermal expansion behavior and mechanical stability of the coatings [10,11].

The deposition process is sensitive to processing parameters. Sreekumar and Rao [12] optimized APS conditions, including the plasma torch input power, powder feed rate, stand-off distance, and the torch travel speed of depositing Al_2O_3–40 wt.% TiO_2 coatings on stainless steel substrates with reduced porosity and improved microhardness. Yugeswaran et al. [13] clarified a critical plasma-spraying parameter (CPSP), which can be defined as the ratio of plasma power to primary gas flow rate. Furthermore, the gas flow rate correlates with the in-flight temperature of the powder particles and influences the resulting crystallinity and phase distribution in the produced coating. Alternative methods, such as detonation gun spraying [6] and supersonic plasma spraying [2], produce distinct microstructural features for the coating, while post-treatment processes such as laser remelting further refine the coatings by reducing porosity and promoting grain refinement [14].

Recent achievements include the development of multilayer and bilayer coatings. Eraslan et al. [11] demonstrated that a four-layer Al_2O_3-TiO_2 multilayer coating sintered at 1000 °C exhibits optimal wear strength and corrosion resistance due to decreased porosity and a more homogeneous microstructure. The corrosion current densities of the Al_2O_3-TiO_2 coatings varied from 0.6 to ~6.0 $\mu A/cm^2$. Laser surface engineering methods, as applied by Zhao et al. [15], can modify the crystal structures of the surface through phase transformations and grain refinement, further enhancing the wear resistance. Metal doping strategies have been investigated to mitigate the inherent brittleness of these coatings. Hanifi et al. [16] showed that incorporating 20 wt.% NiAl into an Al_2O_3–40 wt.% TiO_2 (AT40) coating significantly improves fracture toughness and reduces crack potential, thus improving wear performance. For polymer-based substrates, Cong Wang et al. [17] highlighted that the proper dispersion of TiO_2 within the alumina matrix is crucial to achieve favorable tribological and erosion resistance. Furthermore, Chang et al. [18] produced a triple Al_2O_3-ZrO_2-TiO_2 coating via APS that showed a dense microstructure with refined crystalline phases, contributing to improved mechanical properties and resistance to thermal shocks.

Post-deposition modifications further enhance coating performance. Lu et al. [14] applied laser remelting to plasma-sprayed Al_2O_3-40 wt.% TiO_2 coatings, inducing phase transformations (e.g., a shift from $TiAl_2O_5$ to a mixture of Al_2O_3 and Ti_3O_5) and grain refinement that reduce friction coefficients and wear rates. Lv et al. [19] advanced the coating system by incorporating carnauba wax through a vacuum impregnation process, producing a self-lubricating composite coating with high corrosion resistance. Girisha et al. [20] demonstrated that plasma-sprayed Al_2O_3-40 wt.% TiO_2 coatings on martensitic stainless steel exhibit significantly improved slurry erosion resistance due to their high hardness and low porosity.

Further supporting studies have investigated oxidation behavior and phase stability under harsh conditions. Sharma and Kazi [21] examined the oxidation behavior of detonation-gun-sprayed Al_2O_3-3 wt.% SiC coatings on stainless steel, while Łatka et al. and Lu et al. [22,23] explored the effects of the plasma spray process parameters on oxide phase formation in ceramic coatings. Wang, Qu and Su [24] investigated microstructural changes and phase transformations in plasma-sprayed Al_2O_3-TiO_2 coatings subjected to high-temperature influence. Nguyen et al. [25] evaluated the impact of post-treatment on microstructure and corrosion resistance. Finally, the works by Yu et al. [26] and Kawase et al. [27] explored the relationship between the coating microstructure and long-term performance in various corrosive environments. Y. Wang et al. [28] observed that the corrosion resistance of the Al_2O_3-13wt.% TiO_2 coatings could be controlled by the nature of the feedstock powders used. The corrosion current densities depended on the porosity, pore size, density and phase composition of the coatings. E. Celik et al. [29] demonstrated that the corrosion rate of the Al_2O_3-TiO_2 coatings increased with the increase in the porosity. The current density was from 153 to 485 A/cm^2, depending on the porosity values of the coatings. Our previous investigations [30,31] indicated that the phase composition and morphology of the Al_2O_3 and Al_2O_3-TiO_2 coatings depend on the power of the plasma torch. In biomass combustion systems, the formation of potassium, sodium, and chlorine compounds in flue gases leads to aggressive reactions on the surfaces of the furnace. In particular, chlorine is released as HCl and Cl_2, which react with the heated fire grate surfaces to trigger severe active oxidation, significantly shortening the service life of conventional metallic grates. The deposition of ceramic coatings on metal substrates is proposed as a promising solution to improve the durability of fire grates.

In summary, the quality of plasma-sprayed Al_2O_3-TiO_2 coatings depends on the interaction between chemical composition, crystallographic processes, coating processing parameters, and post-treatment conditions. Optimizing the TiO_2 content and properly controlling the plasma spray conditions are essential to refining the structure of coatings to improve wear, corrosion, and thermal resistance. The present study aims to deposit Al_2O_3, Al_2O_3-3 wt.% TiO_2, Al_2O_3-13 wt.% TiO_2, and Al_2O_3-40 wt.% TiO_2 coatings using a DC air–hydrogen plasma-spraying technology and to investigate the effects of corrosion and thermal impact on the microstructure and phase composition. These investigations are important for developing ceramic coatings capable of significantly extending the lifetime of fire grates in biomass-fired furnaces and other devices operating in corrosive environments.

2. Experimental Setup, Materials and Methods

In this work, the alumina feedstock was combined with titania in different proportions to generate four types of coatings: pure Al_2O_3, Al_2O_3-3 wt.% TiO_2, Al_2O_3-13 wt.% TiO_2, and Al_2O_3-40 wt.% TiO_2. The coatings were deposited on P265GH steel substrates under atmospheric pressure conditions using a direct current (DC) plasma torch developed at the Lithuanian Energy Institute (Kaunas, Lithuania) [4,30,31]. P265GH is a low alloy steel with a chemical composition according to the European standard (EN 10028-2) of approximately C: 0.16–0.18 wt.%, Mn: 0.5–1.0 wt.%, Si: 0.20–0.40 wt.%, P: $\leq$0.025 wt.%, S: $\leq$0.025 wt.%. The DC plasma torch operates with a stable electric arc generated between a hot-button-type hafnium cathode and a high-purity copper anode. In this research, air was used as both the primary plasma-forming gas and the powder-carrying gas. When the airflow passes through the ignited electric arc, a high-temperature, high-speed plasma flow is generated. The inherent versatility of the DC plasma-spraying method is its ability to generate high-temperature flows, which allows for effective melting and deposition of high-melting-point ceramic powder. The DC plasma generator is intensively water-cooled to protect the electrodes and maintain process stability.

Figure 1 illustrates a schematic diagram of the experimental setup, which consists of the plasma torch and the reactor. The reactor is a water-cooled stainless-steel tube measuring 150 mm long with a 7 mm internal diameter and channels for hydrogen gas and raw powder inlet. A hydrogen inflow channel is 100 mm from the outlet nozzle. The hydrogen gas flow increases the thermal energy of the plasma jet, thereby ensuring that the injected powders reach the desired fully molten state.

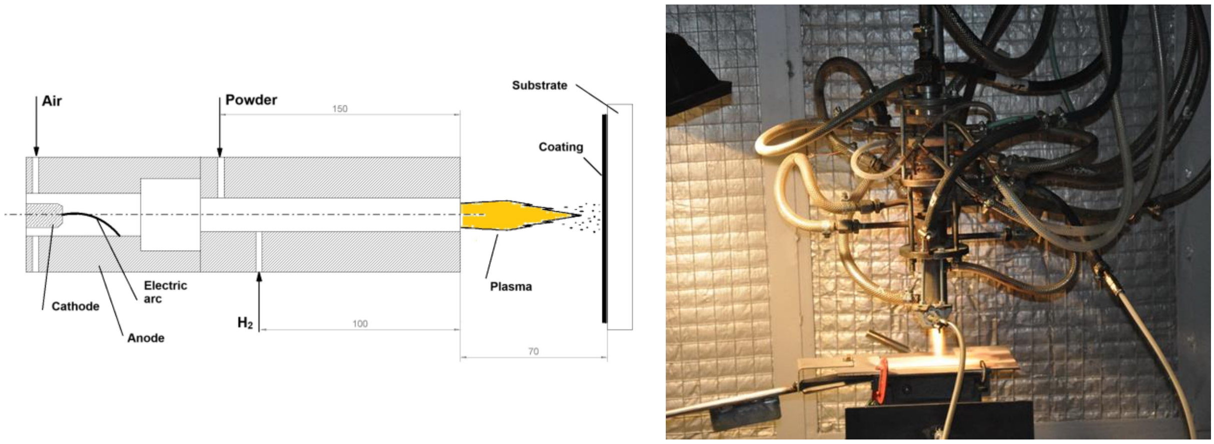

(**a**) (**b**)

Figure 1. Experimental setup of plasma spraying. (**a**) Schematic diagram of a DC plasma torch used for plasma spraying, (**b**) plasma torch in the process.

Before deposition, the steel substrates (40 mm × 10 mm × 6 mm) were pretreated prior to the coating process. They were pretreated by steel grit blasting to enhance surface roughness and remove surface contaminants such as rust and mill scale from the surface, ground and polished with sandpaper (60 grit) to remove surface irregularities, and then thoroughly cleaned by sequential washing in acetone and ethanol to eliminate contaminants. The deposition parameters are listed in Table 1 and include an arc current of 200 A, a voltage of 203 V, a mean plasma jet temperature of 3200 K, and a jet speed of 1060 m/s, when the primary gas flow rates, powder carrier gas, and secondary hydrogen gas were 4.2 g/s, 0.75 g/s, and 0.06 g/s, respectively. The spray distance was maintained at 70 mm. The entire spraying process, while moving a plasma torch horizontally forward and back, was completed in 60 s. A thin nickel–chromium bonding layer (Ni/Cr ratio of 80/20, MOGUL M3, size 105/45 µm) was first deposited onto the substrate using the same plasma spray process before deposition of the main ceramic coating to improve adhesion of the coating. The bonding layer was formed by passing through the steel substrate twice (backward and forward). Dried hard spherical powders were used for coating spraying. The feedstock consisted of a conventional Al_2O_3 powder (particle size ~63 µm, MOGUL PC15, 99.8% purity) and an Al_2O_3 powder mixed with 3 wt.%, (MOGUL PC10), 13 wt.% (MOGUL PC12) or 40 wt.% TiO_2 (MOGUL PC14, MOGUL METALLIZING GmbH, Kottingbrunn, Austria). The resulting ceramic coatings exhibited a uniform thickness between 50 and 65 μm, with an underlying Ni/Cr bond layer of approximately 15–20 μm.

Table 1. Plasma-spraying conditions for the deposition of ceramic coatings.

Arc Current	Voltage	Mean Plasma Jet Temperature	Mean Plasma Jet Speed	Spray Distance	Primary Gas Flow Rate	Powder Carrier Gas Flow Rate	Secondary Gas Flow Rate	Spray Duration
200 A	200–203 V	3200 K	1060 m/s	70 mm	4.2 g/s	0.75 g/s	0.06 g/s	60 s

The surface morphology of the Al_2O_3 and Al_2O_3–TiO_2 coatings was examined by scanning electron microscopy (SEM) using a Hitachi S-3400N instrument (Hitachi, Tokyo, Japan). Energy-dispersive X-ray spectroscopy (EDS) was used to carry out elemental composition and distribution analyses (Bruker Quad 5040 spectrometer, Bruker Nano GmbH, Hamburg, Germany). The elemental data of each sample were obtained by EDS scanning a 1.05 mm^2 area at four different locations, and the mean values of these measurement values were reported. To investigate the crystalline phases of the coatings, X-ray diffraction (XRD) was performed on a Bruker D8 system (Bruker, Hamburg, Germany) using CuKα radiation (λ = 0.154059 nm) over a 2θ range of 20 to 70°.

Thermal and corrosive resistance tests of the coating samples produced were carried out at 500 °C using a 35% KCl solution. A defined volume of the KCl solution was applied to the coatings at the beginning of the test cycle. After that, the samples were kept at 500 °C in a controlled furnace environment for 1 h. The experiment was repeated five times. After each cycle, the samples were rinsed with distilled water in an ultrasonic bath, dried, and then examined to evaluate changes in the coating's surface morphology and elemental composition.

Corrosion tests were performed in a naturally aerated 0.5 mol/L sodium chloride (NaCl) aqueous solution at 22 ± 1 °C. A BioLogic® SP-150 potentiostat-galvanostat (Seyssinet-Pariset, Grenoble, France), interfaced with a personal computer for control and data acquisition, was used for all electrochemical measurements. Two electrochemical techniques were employed: (1) long-term (up to 96 h) open-circuit or steady-state potential measurements (chronopotentiometry), and (2) linear polarization (potentiodynamic) measurements at fixed time intervals (1 h, 12 h, 24 h, 48 h, 72 h, and 96 h) after sample immersion in the corrosive medium. For each test time interval, the potentiodynamic method was applied using a new sample obtained under identical conditions. The electrochemical tests were performed in a 150 mL glass three-electrode cell. The working electrode was the sample itself, with an exposed surface area of 1 cm^2 (the remaining area was insulated with epoxy resin). A platinum (Pt) plate with a surface area of 10 cm^2 served as the counter electrode, and a saturated Ag/AgCl electrode (E = 0.197 V vs. SHE) filled with a saturated aqueous potassium chloride (KCl) solution was used as the reference electrode.

The potentiodynamic polarization curves were recorded in a range of no less than ±180 mV around the open circuit potential, starting with cathodic polarization and the sweeping electrode potential in the anodic direction at a scan rate of 0.166 mV/s using BioLogic® software EC-Lab V10.39. The Tafel equation constants β_a and β_c, which describe the kinetics of the anodic and cathodic corrosion processes, were determined from the potentiodynamic curves. These values facilitated the identification of the rate-controlling corrosion process (anodic or cathodic) and enabled the calculation of corrosion parameters: the corrosion potential ($E_{corr.}$) and the corrosion current density ($i_{corr.}$).

3. Results and Discussion

3.1. The Morphology of Deposited Coatings

For the formation of the plasma-sprayed coatings, the following ceramic materials were used as raw powders: Al_2O_3 (MOGUL PC15, 99.8% purity) with an average particle size of 63 µm; Al_2O_3–3% TiO_2, (MOGUL PC10 (Al_2O_3/TiO_2 ratio 97/3, 63 µm); Al_2O_3–13% TiO_2 (MOGUL PC12, Al_2O_3/TiO_2 ratio 87/13, 63 µm); Al_2O_3–40% TiO_2 (MOGUL PC14, Al_2O_3/TiO_2 ratio 60/40, 63 µm) (the raw powders can be seen in Figure 2a–d). The images show that the raw powder particles were angular in shape and of varying sizes, with an average diameter ranging from 20 to ~70 µm.

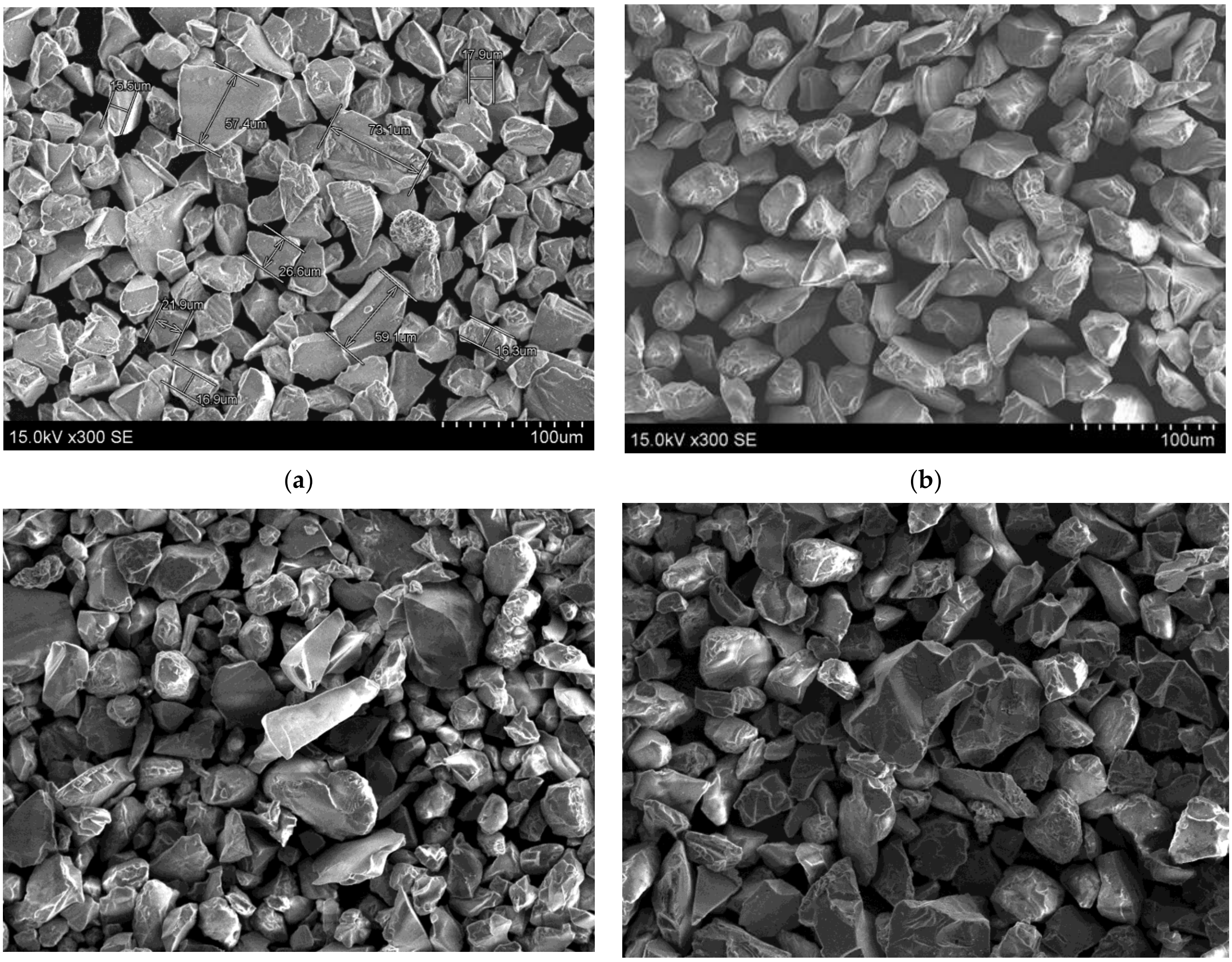

(**a**) (**b**)

(**c**) (**d**)

Figure 2. SEM images of raw powders used for coating formation: (**a**) Al_2O_3 (**b**) Al_2O_3–3% TiO_2, (**c**) Al_2O_3–13% TiO_2, (**d**) Al_2O_3–40% TiO_2.

All coatings were deposited on metal substrates made from P265GH steel, which is commonly used for pressure vessel and boiler applications. To ensure adequate adhesion between the metallic substrate and the ceramic coating, an intermediate metallic bond layer was applied using the Ni/Cr powder. To protect the steel substrate from high temperatures during plasma spraying and ensure a strong adhesion in all coated samples, the substrate was placed on the water-cooled holder, and a copper paste was applied to the backside of the substrate plate to enhance heat dissipation. This controlled cooling strategy minimizes thermal stress and prevents overheating of the substrate, thus improving the adhesion quality of the subsequent ceramic coating. After the coating deposition process, the coating microstructure, surface morphology, and elemental composition were analyzed (Figure 3a–d). A higher input power of the plasma torch gradually reduces the surface roughness, and the smoothest coatings surfaces are obtained using a plasma torch power of not less than 40 kW due to more particles being fully melted. The molten particles demonstrate lower viscosity values at higher temperatures, and a less viscous liquid is more likely to splash [25,27,31].

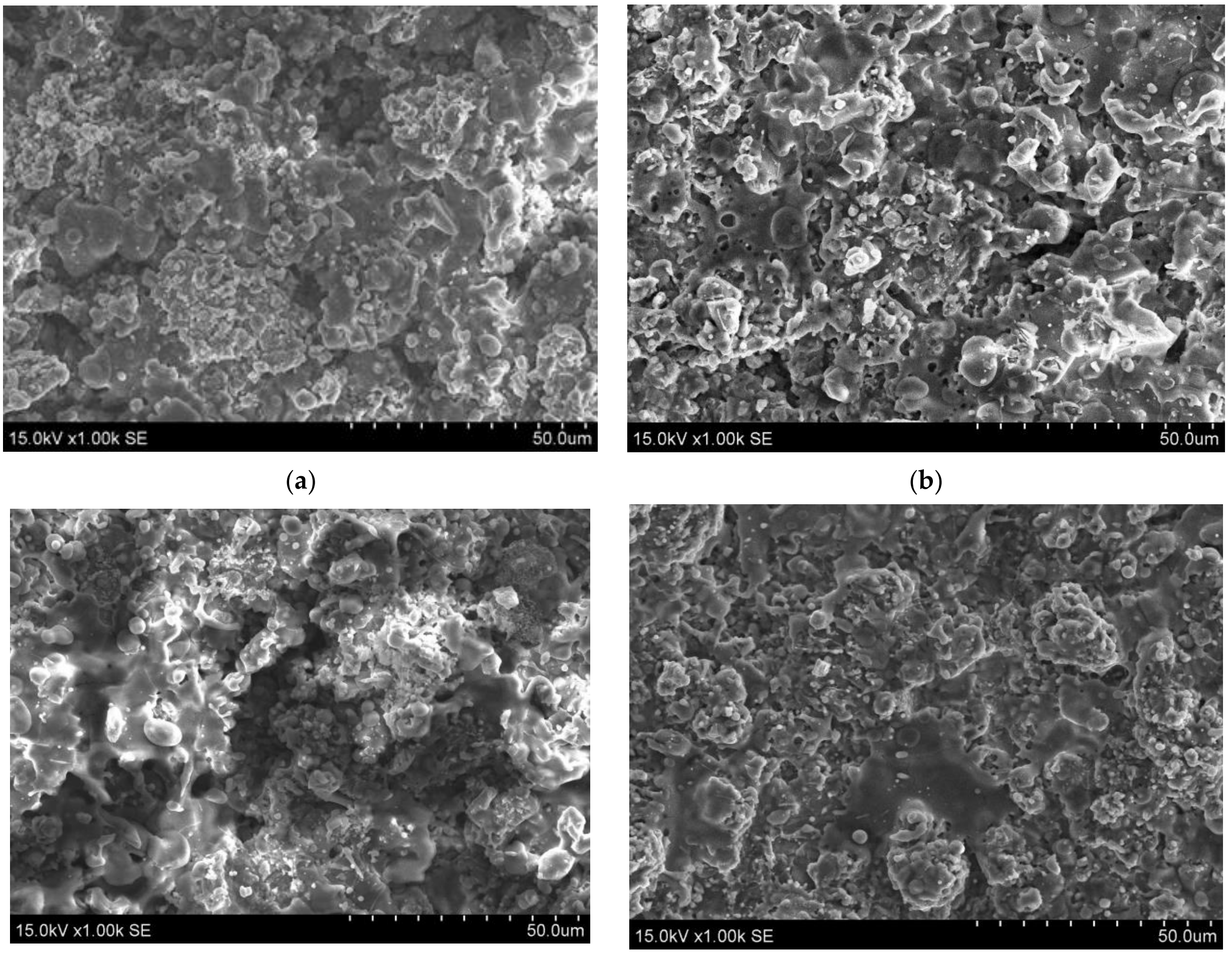

(**a**) (**b**)

(**c**) (**d**)

Figure 3. Surface morphology of coatings produced by plasma spraying: (**a**) Al_2O_3 coating; (**b**) Al_2O_3 + 3% TiO_2; (**c**) Al_2O_3 + 13% TiO_2; (**d**) Al_2O_3 + 40% TiO_2.

SEM analysis revealed that all of the coatings exhibit a uniform morphology, with no observable defects or cracks. After deposition, EDS and XRD analyses were performed to evaluate the coatings' elemental composition, phase composition, and crystallographic structure.

The coating, deposited using the Al_2O_3 powder on a steel substrate with a NiCr bond layer, consists primarily of aluminum (36 ± 1 at.%) and oxygen (60 ± 3 at.%). It also contains minor amounts of carbon (1.0 ± 0.2 at.%) and copper (1.0 ± 0.2 at.%), along with elements originating from the bond layer, namely, nickel (1.4 ± 0.2 at.%) and chromium (0.4 ± 0.1 at.%). In the Al_2O_3 coating XRD pattern, the most intense peaks correspond to the γ-Al_2O_3 phase (at 37.7°, 39.5°, 45.9°, 60.8°, and 67.0°), card No. 75-921, and the α-Al_2O_3 phase (at 25.6°, 35.2°, 37.8°, 43.4°, 52.6°, 57.6°, 66.7°, and 68.3°), card No. 83-2080 (see Figure 4, red line). The presence of the Ni/Cr compound is indicated by peaks around 44.2° and 51.5° (card No. 01-071-7595), while peaks observed at 36.6° and 42.3° suggest the formation of copper oxide.

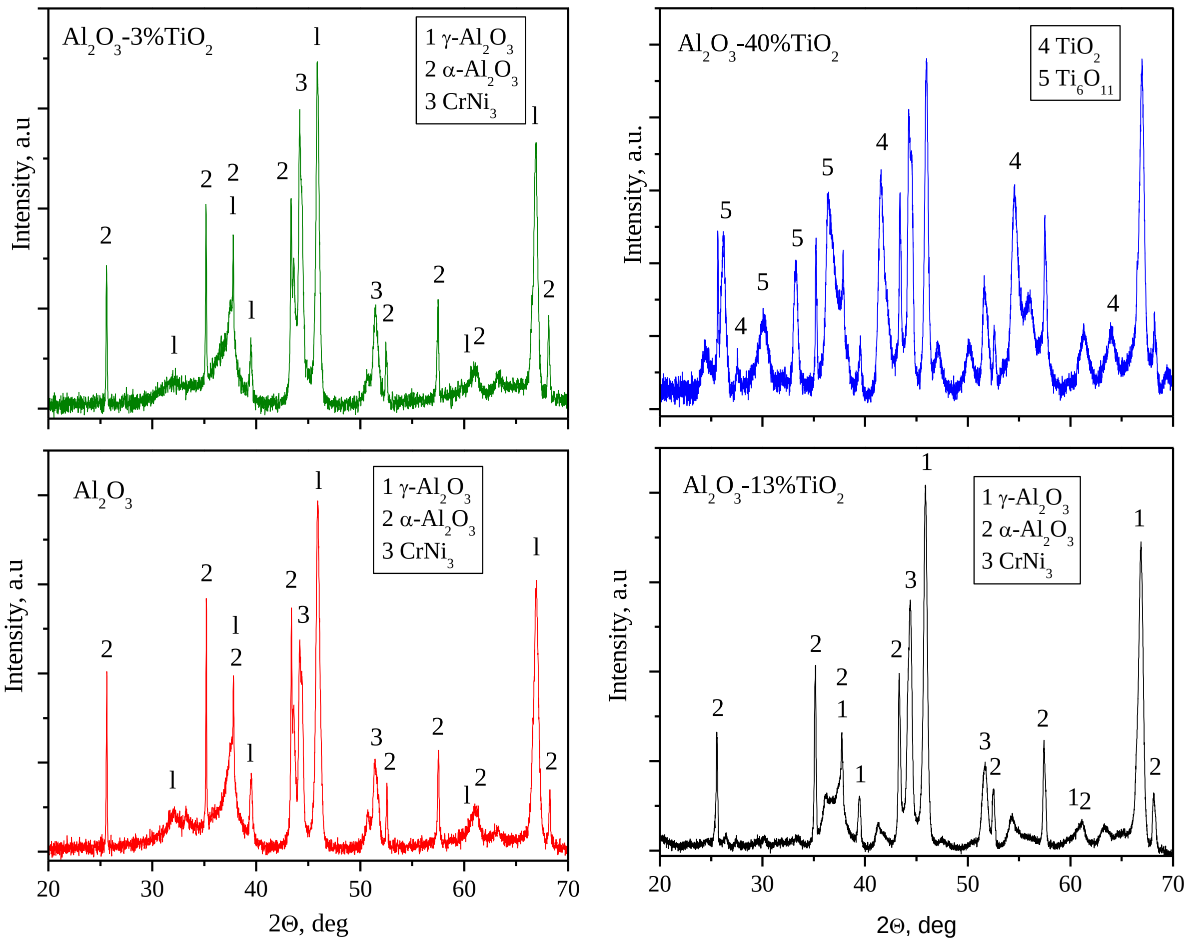

Figure 4. XRD analysis results of coatings produced by plasma spraying: (red)—Al_2O_3 coating; (green)—Al_2O_3–3% TiO_2; (black)—Al_2O_3–13% TiO_2; (blue)—Al_2O_3–40% TiO_2.

The coating deposited from Al_2O_3–3 wt.% TiO_2 powder (using a NiCr bond layer) on a P265GH substrate is composed of aluminum (32 ± 2 at.%), oxygen (58 ± 3 at.%), titanium (1.7 ± 0.2 at.%), nickel (4.0 ± 0.5 at.%), and chromium (1.5 ± 0.1 at.%), with a small amount of carbon (1.0 ± 0.2 at.%), among other elements. X-ray diffraction analysis of the coating produced from the Al_2O_3–3 wt.% TiO_2 powder revealed that the dominant crystalline phases are γ-Al_2O_3 and α-Al_2O_3. The γ-Al_2O_3 phase is indicated by peaks at approximately 37.7°, 39.5°, 45.9°, 60.8°, and 67.0°, while the α-Al_2O_3 phase is evidenced by peaks at 25.6°, 35.2°, 37.9°, 43.4°, 52.6°, 57.6°, 66.7°, and 68.3° (see Figure 4, green line). Furthermore, peaks at around 44.2° and 51.5° confirm the presence of the Ni/Cr compound, and a peak at approximately 44.9° is associated with the steel substrate. The diffraction peaks of the crystalline phases associated with the TiO_2 rutile are detected, though they exhibit a low intensity.

The coating produced from the Al_2O_3–13 wt.% TiO_2 powders (using a Ni/Cr bond layer, a steel substrate) is composed of aluminum (30 ± 1 at.%), oxygen (60 ± 3 at.%), titanium (6.0 ± 0.3 at.%), and a small amount of carbon (1.2 ± 0.2 at.%), along with elements from the bond layer (Ni—1.8 ± 0.2 at.% and Cr—0.4 ± 0.1 at.%). In the XRD pattern of the coating with Al_2O_3–13 wt.% TiO_2, the most intense peaks are attributed to the γ-Al_2O_3 phase (observed at 37.7°, 39.5°, 45.9°, 60.8°, and 67.0°) and the α-Al_2O_3 phase (at 25.6°, 35.2°, 37.8°, 43.4°, 52.6°, 57.6°, 61.2°, and 68.3°) (see Figure 4, black line). The existence of the nickel–chromium compound is confirmed by peaks around 44.2° and 51.5°. Furthermore, broad peaks at 27.5°, 41.3°, and 54.3° indicate the presence of the TiO_2 rutile phase (card No. 00-021-1276), while additional peaks at 26.5°, 30.2°, 33.3°, and 36.2°

are associated with a Ti_6O_{11} compound (card No. 00-018-1401). The coating produced from Al_2O_3–40% TiO_2 powders, using a NiCr bond layer, exhibits the following elemental composition: Al—23 ± 1 at.%, O—50 ± 3 at.%, Ti—24 ± 1 at.%, C—0.7 ± 0.2 at.%, and Ni—1.2 ± 0.2 at.% and Cr—0.6 ± 0.1 at.%. The summarized results of the EDS analysis of the sprayed coatings are presented in Table 2.

Table 2. Summary of the EDS results: elemental composition of the Al_2O_3, Al_2O_3-TiO_2 coatings.

	Samples			
Composition	**Al_2O_3**	**Al_2O_3 + 3%TiO_2**	**Al_2O_3 + 13%TiO_2**	**Al_2O_3 + 40%TiO_2**
Oxygen, at.%	60	58	60	50
Carbon, at.%	1	1	1.2	0.7
Nickel, at.%	1.4	4	1.8	1.2
Chromium, at.%	0.4	1.5	0.4	0.6
Aluminum, at.%	36	32	30	23
Titanium, at.%	-	1.7	6	24
Copper, at.%	1			

XRD analysis indicates that the formed Al_2O_3–40 wt.% TiO_2 coating contains both γ-Al_2O_3 and α-Al_2O_3 phases. The peaks observed at approximately 27.4°, 41.3°, 53.9°, and 64.1° in the XRD pattern are indicative of the TiO_2 rutile phase. Relatively broad and intense peaks at around 26.2°, 30.2°, 33.2°, 41.6°, 47.3°, 50.2°, and 54.6° are associated with the formation of crystalline compounds such as Ti_3O_5 and Al_2TiO_5. Additionally, low intensity peaks near 24° and 29.5° suggest the formation of the $H_2Ti_3O_7$ phase (see Figure 4, blue line). The percentage volume of the alpha-Al_2O_3 and gamma-Al_2O_3 phase in the Al_2O_3 and Al_2O_3-TiO_2 coatings was determined by the methodology presented in [32,33]. The results indicated that the Al_2O_3 coating is composed of 40.8% of α-Al_2O_3 and 59.2% of γ-Al_2O_3 phase. The addition of 3% by weight of TiO_2 in the Al_2O_3 powders resulted in a reduction in the α-Al_2O_3 phase down to 35.8% in the coating. The lowest content (31.0%) of the α-Al_2O_3 phase was observed in the Al_2O_3–13 wt.% TiO_2 coating. A slight increase of up to 35.4% in the α-Al_2O_3 phases was observed in the Al_2O_3–40 wt.% TiO_2 coating. The results showed that the composition of the initial powder determines the different amounts of α-Al_2O_3 and γ-Al_2O_3 phases in the as-sprayed coatings and will also affect the properties of the coatings. It was observed that the increase in the γ-Al_2O_3 phase volume fraction in the Al_2O_3 or Al_2O_3-TiO_2 coatings indicates a higher melting of the Al_2O_3 particle and/or an increased solidification rate of the alumina splats [32,34].

3.2. The Corrosive–Thermal Resistance of Deposited Coatings

After the thermal–chemical treatment at 500 °C with the coatings wetted with KCl solution, etched grooves approximately with a thickness of 2–3 µm were observed on the Al_2O_3-3wt.% TiO_2 coating surface (see Figure 5b). No delamination or macroscopic microcracks were observed. The overall composition remained almost unchanged (Al: 35 ± 1 at.%, O: 60 ± 3 at.%, Ti: 1.3 ± 0.2 at.%), while trace amounts of potassium (1 at.%) and chlorine (0.4 at.%) appeared on the surface.

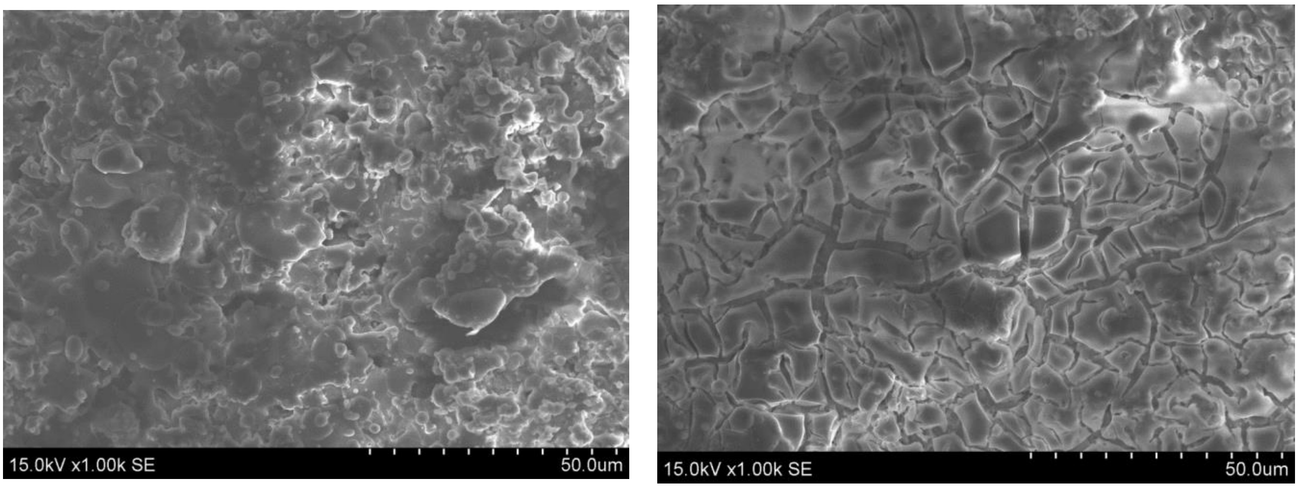

(**a**) (**b**)

Figure 5. Surface images of the Al_2O_3–3 wt.% TiO_2 coating: (**a**) before and (**b**) after chemical treatment.

Using powders of Al_2O_3–13 wt.% TiO_2, the coating was formed from a mixture of microgranules of different sizes (see Figure 6a). Elemental analysis of the as-sprayed coating indicated concentrations of approximately 27 ± 2 at.% aluminum, 58 ± 2 at.% oxygen and 5.5 ± 0.5 at.% titanium. After chemical treatment with a 35% KCl solution, the coating remained almost intact and a few microcracks appeared on the surface (see Figure 6b red arrows). EDS measurements confirmed these observations, showing that the concentrations of the primary coating elements decreased (Al: 18 ± 2 at.%, O: 40 ± 2 at.%, Ti: 3 ± 0.5 at.%), while a significant amount of iron (up to 21 at.%) was detected, along with trace amounts (~1 at.%) of potassium and chlorine.

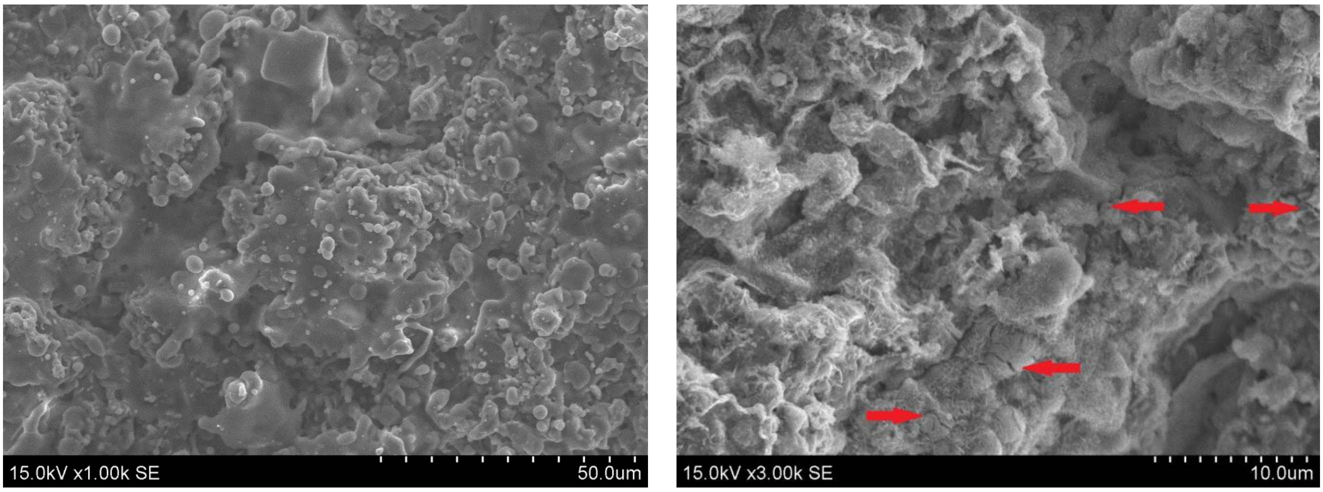

(**a**) (**b**)

Figure 6. Surface images of the Al_2O_3–13 wt.% TiO_2 coating: (**a**) before and (**b**) after chemical treatment. Red arrows indicate the microcracks caused by chemical treatment with 35% KCl.

After chemical treatment with a solution of 35% KCl, it was found that the coating produced from an Al_2O_3–40 wt.% TiO_2 mixture (see Figure 7a) was partially etched. EDS analyses showed that the oxygen concentration decreased from 50 ± 2 at.% to 40–45 at.%, the aluminum concentration dropped from 23.5 at.% to between 4 and 16 at.%, and the titanium concentration decreased from 23.5 at.% to 4–10 at.%. In areas where the coating was completely removed (Figure 7b), microregions with exposed substrate exhibited iron concentrations ranging from 10 at.% to 50 at.%. The coating is not resistant to chemical impact at 500 °C.

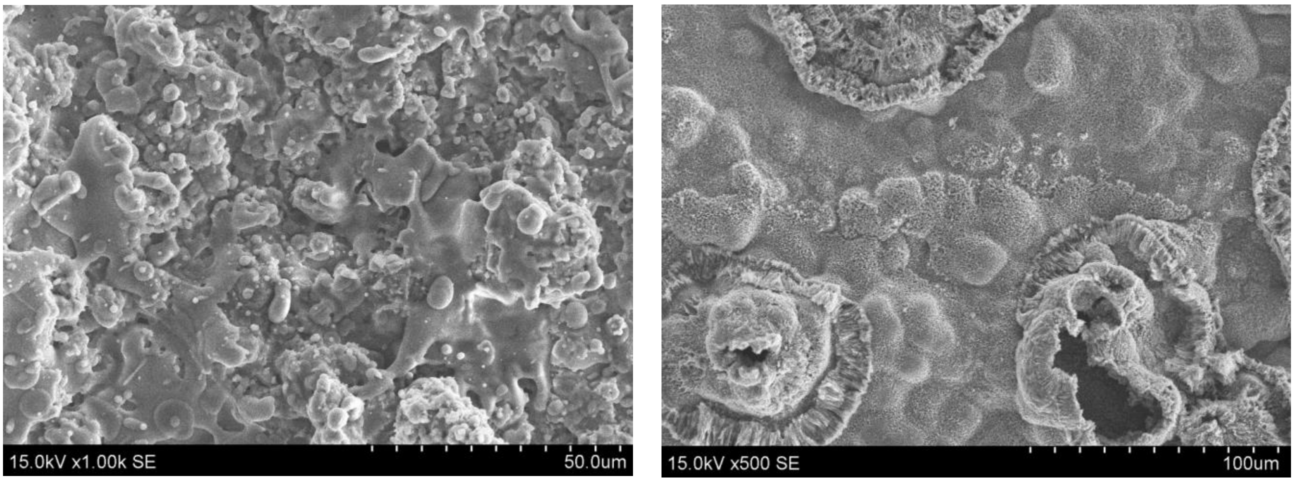

(**a**) (**b**)

Figure 7. Surface images of the Al_2O_3–40 wt.% TiO_2 coating: (**a**) before and (**b**) after chemical treatment.

Chemical resistance tests demonstrated that coatings produced from Al_2O_3 powders with a higher TiO_2 content suffer more severe damage. The least damage was observed in coatings fabricated from pure alumina and alumina with 3% titanium oxide. Although the surface of the coatings is affected, the coating remains intact with no pore formation throughout its thickness. In particular, while the Al_2O_3–40% TiO_2 coating shows resistance to thermal exposure at 500 °C, its high titanium content makes it less resistant to chemical impact. It was indicated that the presence of TiO_2 in the coatings facilitates an ion exchange reaction with potassium and leads to the formation of potassium titanates at higher temperatures [11]. The increase in the titania content could create some additional microchannels for the diffusion of Cl^- or K^+ ions at higher temperatures. As thermal annealing was carried out under atmospheric conditions, the chemical reactions with the metals of bonding layer or the substrate could be induced. The Cr or Fe could start reacting with K and Cl ions, resulting in the formation of volatile compounds. As a result, pitting and spallation on the surface of the coating was induced (Figure 7b).

3.3. The Corrosion Behavior of Deposited Coatings

The corrosion behavior of the deposited coatings was then investigated in a naturally aerated 0.5 mol/L sodium chloride (NaCl) aqueous solution maintained at 22 ± 1 °C. Figure 8 illustrates the evolution of the open-circuit potential (E_{OCV}) as a function of immersion time for different samples: bare steel, steel coated with pure Al_2O_3, steel coated with Al_2O_3–3 wt.% TiO_2, and steel coated with Al_2O_3–13 wt.% TiO_2. The bare steel initially exhibits a relatively high (more positive) potential, which then steadily decreases over the first 12 h (from approximately −380 mV to −625 mV) and stabilizes between −620 and −640 mV between 24 and 96 h. On the contrary, the oxide-coated samples display a distinct behavior. The Al_2O_3–3 wt.% TiO_2 and pure Al_2O_3 coatings quickly reach their most negative potentials (−790 mV and −810 mV, respectively) within the first 6 h, and then shift to less negative values. In particular, the Al_2O_3–13 wt.% TiO_2 coating starts with a comparatively lower potential (approximately −715 mV) but gradually becomes less negative (approximately −580 mV after 96 h). The slight increase in the open-circuit (or free corrosion) potential (their shift toward more positive values) of all coatings over time is most likely related to surface deactivation caused by the formation of a more stable protective layer of corrosion products.

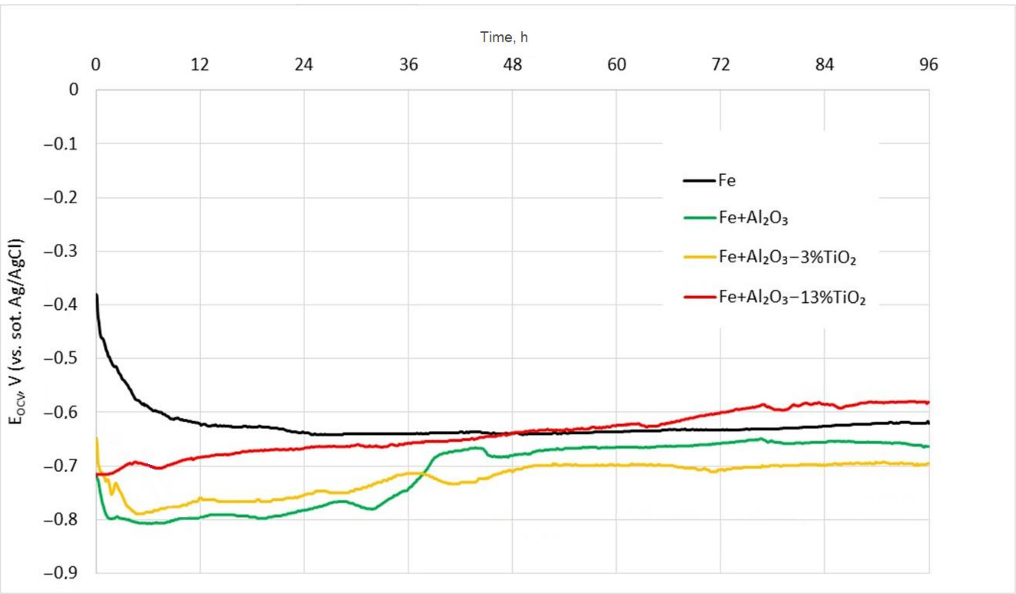

Figure 8. Open-circuit potential (E_{OCV}) vs. immersion time in a naturally aerated 0.5 mol/L NaCl solution at 22 ± 1 °C for bare steel and steel samples coated with Al_2O_3, Al_2O_3–3 wt.% TiO_2, and Al_2O_3–13 wt.% TiO_2.

Table 3 summarizes the key corrosion kinetic parameters determined from the Tafel analysis of the potentiodynamic curves (Figure 9). These include the anodic (β_a) and cathodic (β_c) Tafel slopes, the corrosion potential ($E_{corr.}$), and the corrosion current density ($i_{corr.}$) at various immersion times. The results indicate that while the bare steel corrodes most rapidly at the beginning of immersion, its corrosion rate decreases during the initial 48 h—likely due to the formation of loosely adherent corrosion products—before increasing again. In contrast, oxide coatings exhibit consistently lower corrosion current densities, reflecting their improved barrier properties. The differences in Tafel slopes between the samples further suggest that the corrosion process is controlled by either the anodic or cathodic reactions depending on the type of coating, which correlates with the passivation behavior observed in the OCP measurements.

Table 3. The corrosion kinetic parameters of the steel substrate and the plasma-sprayed coatings on it. Corrosion media: a naturally aerated 0.5 mol/L NaCl solution at 22 ± 1 °C.

Sample	Time, h	$E_{corr.}$, mV	$i_{corr.}$, µA/cm^2	β_a, mV/Decade	β_k, mV/Decade
Fe (substrate)	1	−474.9	23.4	111.5	869.8 **
	12	−643.9	21.6	95.5	454.7 **
	24	−661.4	20.8	97.1	370.9 **
	48	−680.0	15.5	100.6	169.2 **
	72	−678.1	18.2	103.7	140.1 **
	96	−655.3	29.4	104.7	155.5 **

Table 3. *Cont.*

Sample	Time, h	$E_{corr.}$, mV	$i_{corr.}$, μA/cm^2	β_a, mV/Decade	β_k, mV/Decade
Fe + Al_2O_3	1	−756.9	0.6	99.6	121.1 **
	12	−834.3	4.7	222.6 *	133.9
	24	−810.8	5.2	248.9 *	156.5
	48	−687.3	7.8	119.2	184.2 **
	72	−653.3	11.4	130.0	188.9 **
	96	−662.6	8.4	140.7	184.4 **
Fe + Al_2O_3—3%TiO_2	1	−789.1	18.08	429.8 *	158.9
	12	−809.5	18.32	381.7 *	179.4
	24	−790.7	17.80	281.8 *	166.7
	48	−750.0	14.18	346.6 *	163.8
	72	−748.5	16.05	347.6 *	168.4
	96	−725.9	11.67	203.5 *	154.2
Fe + Al_2O_3—13%TiO_2	1	−754.0	12.4	151.9	147.0 *
	12	−697.4	12.8	82.2	149.8 *
	24	−662.1	13.0	68.9	210.8 *
	48	−640.1	13.5	138.3	191.4 *
	72	−608.6	17.3	196.4	231.7 *
	96	−589.1	17.4	118.9	215.2 *

The Tafel slopes indicate the rate-controlling process: * when $\beta_a > \beta_c$, the anodic reaction limits the corrosion rate; conversely, ** when $\beta_c > \beta_a$, the cathodic reaction is the limiting step.

Comprehensive analysis of the potentiodynamic curves, coupled with the time-dependent evolution of E_{OCV} demonstrates that the protective efficacy of the coatings is highly dependent on their microstructural integrity and phase composition. Well-adherent, dense and uniform oxide films provide superior isolation of the underlying steel substrate from the corrosive environment.

Calculations of the corrosion current densities for the various samples (as summarized in Table 3), which are directly proportional to the corrosion rate, and their evolution over time (illustrated in Figure 10), revealed that the bare steel substrate corrodes most rapidly immediately upon immersion in the corrosive medium. During the first 48 h, its corrosion rate decreases by approximately 1.5 times, after which the corrosion current density, and therefore the corrosion rate, increases again. After 96 h, the corrosion rate of the bare steel is approximately 1.25 times higher than that measured one hour after immersion. This behavior is attributed to the formation of a loosely adherent and poorly protective layer of corrosion products (rust) on the steel surface.

The corrosion kinetics of the coatings varied significantly with composition. The pure Al_2O_3 coating corrodes the most slowly immediately after immersion in the corrosive medium. However, during the first 72 h, its corrosion current density increases approximately 19-fold and then slightly decreases by about 1.36 times between 72 and 96 h. In contrast, steel substrates coated with mixed oxide layers (Al_2O_3–3 wt.% TiO_2 and Al_2O_3–13 wt.% TiO_2) exhibit initial corrosion rates that are approximately 1.3 and 1.9 times lower, respectively, compared to uncoated steel. Over time, the evolution of the corrosion current density differs between these coatings: after 96 h, the Al_2O_3–3 wt.% TiO_2 coating shows a uniform decrease in the corrosion current density by approximately 1.55 times, while the Al_2O_3–13 wt.% TiO_2 coating exhibits an increase of approximately 1.4 times. Despite the variation in the corrosion current density of all the investigated coatings over time, the Al_2O_3 coatings on the steel showed the best results during the entire test period (96 h) compared to the steel substrate coated with Al_2O_3-TiO_2. These differences are likely due to variations in the microstructure and phase composition of the mixed oxide coatings.

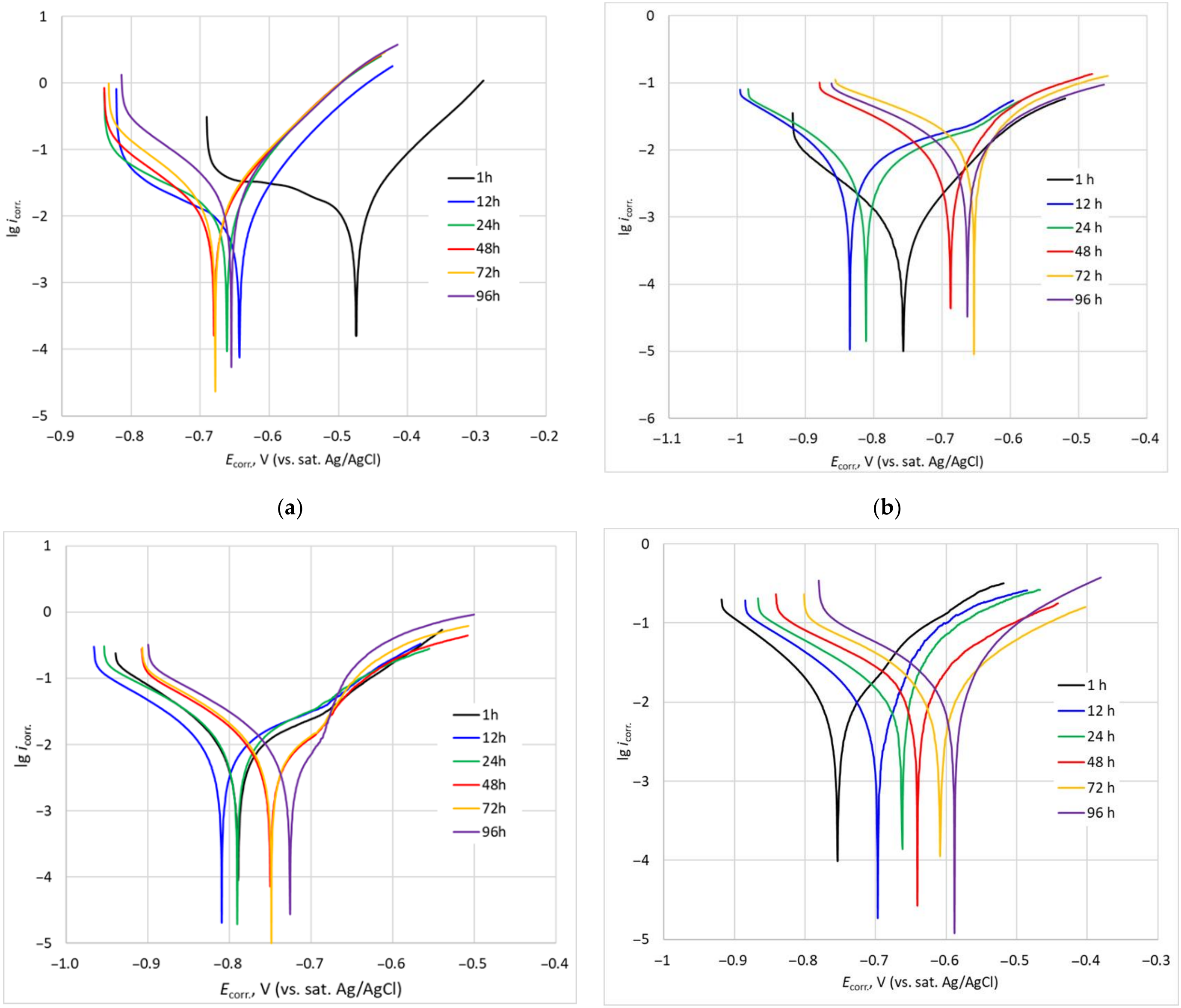

(**a**) (**b**)

(**c**) (**d**)

Figure 9. Potentiodynamic polarization curves obtained after different immersion times in a naturally aerated solution of 0.5 mol/L NaCl at 22 ± 1 °C for bare steel (**a**) and steel samples coated with Al_2O_3 (**b**), Al_2O_3–3 wt.% TiO_2 (**c**), and Al_2O_3–13 wt.% TiO_2 (**d**). The scanning rate of the potential was 0.166 mV/s.

It is well established that oxide coatings on steel act primarily as physical barriers rather than providing intrinsic electrochemical protection. In a neutral aqueous environment (pH~7), neither Al_2O_3 nor TiO_2 oxidize; only cathodic reactions occur on their surfaces (e.g., oxygen reduction that forms hydroxide ions), while anodic oxidation of iron takes place on the exposed steel substrate. Consequently, the protective effect of such coatings depends largely on their quality: dense, smooth, and crack-free cathodic layers offer better protection than those exhibiting more pronounced surface defects or microcracks. The higher corrosion resistance of Al_2O_3 coatings could be related to its chemical stability and less reactivity to potassium chloride compared to Al_2O_3-TiO_2 coatings. TiO_2 typically demonstrates a higher probability to react with NaCl or KCl and forms corrosive compounds [7,28,29,35–37].

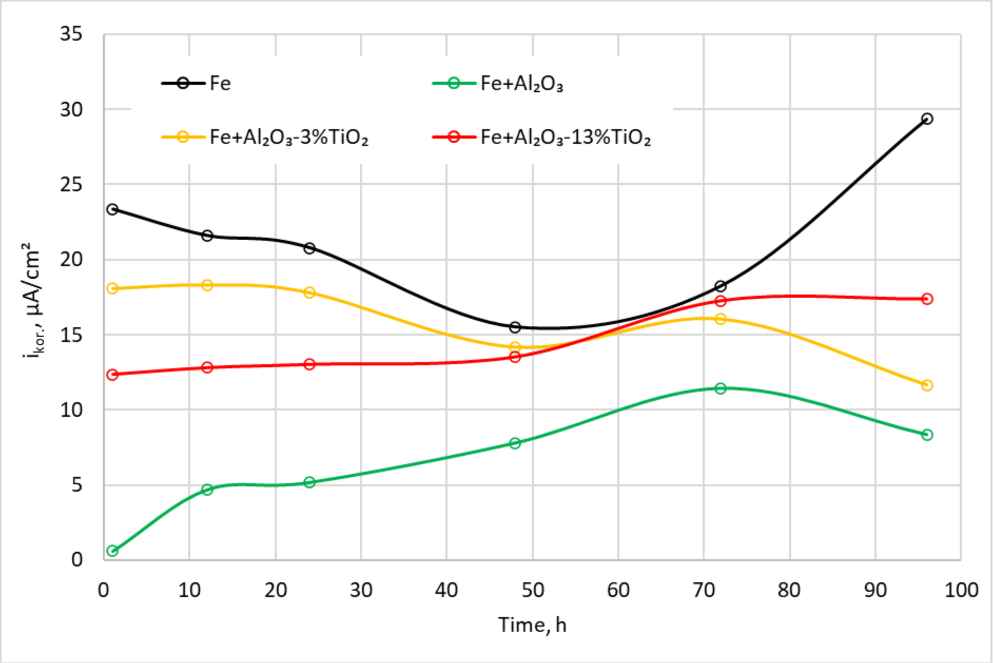

Figure 10. Time-dependent variation in the corrosion current density ($i_{corr.}$. for uncoated steel and various coatings in a naturally aerated 0.5 mol/L NaCl aqueous solution at 22 ± 1 °C.

F.S. Eraslan et al. [11] indicated that the corrosion properties of the Al_2O_3-TiO_2 coatings depended on the number of layers and the sintering temperature. As the layer number increased from 2 to 4, the current density was reduced from ~6.0 $\mu A/cm^2$ to 0.8 A/cm^2, respectively. However, the current density was increased to 3.9 $\mu A/cm^2$ when the six-layer coating was formed. The authors indicated that the increase in microcracks in the Al_2O_3-TiO_2 coatings enhanced the density of the corrosion current. A. Hakimizad et al. [38] reported that the corrosion current densities of the alumina coatings were from 20% to 65% lower compared to those of the alumina–titania coatings. The increase in coating porosity, the formation of a large amount of micro-cracks, and the surface morphology were the main reasons for the enhancement in the corrosion rates. Y. Wang et al. [28] demonstrated that the corrosion resistance of the Al_2O_3-13wt.% TiO_2 coatings depended on the type of feedstock powders used. Corrosion resistance was improved with the formation of more dense and less porous coatings. T. Bayram et al. [37] observed that the plasma-sprayed TiO_2, Al_2O_3 and Al_2O_3-3 wt.% TiO_2 coatings had corrosion currents of 30.1 μA, 9.1 μA, and 2.4 μA, respectively. The lowest corrosion current values were attributed to the formation of the Al_2TiO_6 phase in the Al_2O_3-TiO_2 coating. The investigation of plasma-sprayed mixed-glass-doped Al_2O_3-13 wt.%TiO_2 and pure Al_2O_3-13 wt.%TiO_2 coatings showed that the addition of 10% of the glass mixture resulted in a reduction in porosity of up to 42% and drastically reduced the corrosion current density from 26.9 $\mu A/cm^2$ to 2.1 $\mu A/cm^2$. The improvement in the corrosion resistance of the coating was related to the reduced number of defects (pores and microcracks) due to the formation of a more dense and compact coating [36]. F.S. Eraslan et al. [7] observed that the corrosion resistance of the alumina–titania coatings could be controlled by the weight of TiO_2 in the alumina powders. E. Celik et al. [29] found that the corrosion current densities of the as-sprayed Al_2O_3 and Al_2O_3-TiO_2 coatings were 15.1 A/cm^2 and 267.4 A/cm^2, respectively. The resistance to corrosion was improved due to reduction in the porosity of the Al_2O_3 coating and enhancement in the gamma phase fraction. The higher corrosion resistance of the Al_2O_3 coatings could be related to their chemical stability and less reactivity to sodium chloride compared to the Al_2O_3-TiO_2 coatings. TiO_2 usually shows a higher probability of reacting with NaCl and forming corrosive compounds [37]. It should be noted that higher β_a values are related to thicker coatings with a dense and more compact microstructure [38]. This may lead to a decrease in the depth of penetration of Cl^- ions and suppress the corrosion rate of the coatings. This is likely to have happened in the case of the Al_2O_3 coating, where the corrosion current densities were the lowest and, in some cases, quite high β_a values were achieved (after 12 and 24 h). Additionally, the presence of TiO_2 in the Al_2O_3 coatings could induce some microcracks in the coatings. These microcracks act as channels for aggressive anions, such as Cl− ions, to migrate to the bonding layer and enhance the corrosion rate [28,29,36]. As a result, the corrosion current densities of the Al_2O_3-3wt.% TiO_2 and Al_2O_3-13wt.% TiO_2 coatings were higher compared to the Al_2O_3 coating (Table 3). The stable and quite low corrosion current densities (12.4–13.5 $\mu A/cm^2$) obtained for Al_2O_3-13wt.% TiO_2 up to 48 h could be due to a reduction in the porosity of the coatings. As the melting temperature of TiO_2 is lower compared to that of the Al_2O_3 powders, the increase in the TiO_2 content results in the formation of more dense and lower porosity coatings, which could compensate for a slight increase in the number of microcracks obtained in the Al_2O_3-13wt.% TiO_2 coating. Additionally, the Al_2O_3-13wt.% TiO_2 coating had the lowest content of the α-Al_2O_3 phase, which is a direct indication that the melting degree of the feedstock powders was enhanced and could lead to a reduction in the porosity of the coatings [10,32,34].

4. Conclusions

The present investigation confirms that the corrosion and thermal resistance of plasma-sprayed Al_2O_3–TiO_2 coatings are strongly influenced by their chemical composition and the resulting microstructure. SEM and EDS analyses revealed that the coatings deposited using pure Al_2O_3 or Al_2O_3 with 3 wt.% TiO_2 maintain a uniform, crack-free morphology, which is essential to provide an effective physical barrier against corrosive media. XRD analysis shows that these coatings predominantly consist of γ-Al_2O_3 and α-Al_2O_3 phases. The highest α-Al_2O_3 phase volume of 40.8% was obtained for the Al_2O_3 coating. The weight percentage of the TiO_2 in the alumina matrix allows us to control the phase composition of the as-sprayed coatings. In contrast, coatings with a higher TiO_2 content (13 wt.% and 40 wt.%) exhibit additional crystalline phases such as Ti_3O_5 and Al_2TiO_5, which, while enhancing thermal stability, appear to compromise chemical resistance under aggressive conditions, as evidenced by increased corrosion current densities and micro-scale defects after exposure to 35% KCl at 500 °C. These findings align with previous studies that indicate that the oxide coatings function primarily as physical barriers and that protective efficacy is largely dependent on the coating density, porosity, and integrity. The differences in corrosion kinetics observed between the various compositions underscore the importance of optimizing the TiO_2 content to balance thermal and chemical resistance.

Future research should focus on improving the plasma-spraying parameters and on the use of agglomerated feedstock powders for the deposition of coatings to enhance density and produce less porous coatings. This would allow for a wider application of Al_2O_3 and Al_2O_3-TiO_2 coatings to protect metal surfaces in liquid media from corrosion and wear.

Author Contributions: Conceptualization, V.G., L.M. and A.Š.; data curation, V.G., L.M. and A.Š.; formal analysis, L.M., V.G. and E.G.; investigation, L.M., R.K., A.Š., V.G. and E.G.; methodology, V.G., L.M., A.Š., R.K. and E.G.; supervision, L.M. and V.G.; writing—original draft, V.G., L.M. and

A.Š.; writing—review and editing, V.G., L.M. and A.Š.; visualization, V.G. All authors have read and agreed to the published version of the manuscript.

Funding: This research received no external funding.

Data Availability Statement: The authors confirm that the data supporting the findings of this study are available within this article.

Conflicts of Interest: The authors declare no conflicts of interest.

References

1. Wang, Y.; Jiang, S.; Wang, M.; Wang, S.; Xiao, T.D.; Strutt, P.R. Abrasive wear characteristics of plasma sprayed nanostructured alumina/titania coatings. *Wear* **2000**, *237*, 176–185. [CrossRef]
2. Samal, S. Thermal plasma technology: The prospective future in material processing. *J. Clean. Prod.* **2017**, *142*, 3131–3150. [CrossRef]
3. Tankal, K.; Güney, B.; Erden, M.A. A comparative study of thermal sprayed Al_2O_3-TiO_2 coatings on PM AISI 316L. *Eng. Sci. Technol. Int. J.* **2024**, *60*, 101895. [CrossRef]
4. Valincius, V.; Krusinskaite, V.; Valatkevicius, P.; Valinciute, V.; Marcinauskas, L. Electric and thermal characteristics of the linear, sectional dc plasma generator. *Plasma Sources Sci. Technol.* **2004**, *13*, 199–206. [CrossRef]
5. Brinkiene, K.; Kezelis, R. Effect of alumina addition on the microstructure of plasma sprayed YSZ. *J. Eur. Ceram. Soc.* **2005**, *25*, 2181–2184. [CrossRef]
6. Brar, S.S.; Brar, G.S.; Chawla, V. Characterization of D-gun sprayed Al_2O_3-13%TiO_2 and Al_2O_3-40%TiO_2 coatings on ASTM 316 boiler steel and their microstructure. *Mater. Today Proc.* **2021**, *50*, 2299–2306. [CrossRef]
7. Eraslan, F.S.; Gecu, R. Chemical composition optimization of Al_2O_3-TiO_2 composite coatings for enhanced wear and corrosion resistance. *Surf. Coat. Technol.* **2023**, *474*, 130053. [CrossRef]
8. Ghazali, M.J.; Forghani, S.M.; Hassanuddin, N.; Muchtar, A.; Daud, A.R. Comparative wear study of plasma sprayed TiO_2 and Al_2O_3-TiO_2 on mild steels. *Tribol. Int.* **2016**, *93*, 681–686. [CrossRef]
9. Wei, Z.; Hong, S.; Wei, Z.; Hu, N.; Ying, G.; Wu, Y. Comparison on long-term corrosion performance of WC-CoCr and Al_2O_3-TiO_2 ceramic coatings in sulphide-containing 3.5 wt% NaCl solution. *Int. J. Refract. Met. Hard Mater.* **2022**, *107*, 105906. [CrossRef]
10. Lan, W.; Chen, Z.; Zhang, X.; Bi, W.; Liu, W. Corrosion resistance analysis of Al_2O_3-TiO_2 composite ceramic coatings on carbon steel pipe surfaces. *Alex. Eng. J.* **2025**, *110*, 377–385. [CrossRef]
11. Eraslan, F.S.; Turu, I.C.; Ozcan, M.; Birol, B.; Gecu, R. Influence of layer number and sintering temperature on microstructural, tribological, and corrosion behavior of Al_2O_3-TiO_2 multilayer coatings. *Ceram. Int.* **2023**, *49*, 33226–33235. [CrossRef]
12. Sreekumar Rajesh, T.; Venkata Rao, R. Experimental Investigation and Parameter Optimization of Al_2O_3-40% TiO_2 Atmospheric Plasma Spray Coating on SS316 Steel Substrate. *Mater. Today Proc.* **2018**, *5*, 5012–5020. [CrossRef]
13. Yugeswaran, S.; Selvarajan, V.; Vijay, M.; Ananthapadmanabhan, P.V.; Sreekumar, K.P. Influence of critical plasma spraying parameter (CPSP) on plasma sprayed Alumina-Titania composite coatings. *Ceram. Int.* **2010**, *36*, 141–149. [CrossRef]
14. Lu, Y.; Peng, Y.; Shi, Z. Plasma sprayed Al_2O_3–40%TiO_2 coating by laser remelting: Structural evolution, tribological properties and DFT calculation. *Tribol. Int.* **2023**, *189*, 109009. [CrossRef]
15. Zhao, Y.; Lu, M.; Fan, Z.; Yin, Y.; Lin, W.; Huang, H. Laser surface engineering of Ti–6Al–4V with TiO_2/Al_2O_3 composite powder for improved wear resistance. *Smart Mater. Manuf.* **2023**, *1*, 100015. [CrossRef]
16. Hanifi, D.; Hakimi, N.; Ali, R.; Huang, T.; Huma, T.; Bakhshyar, D.; Afzali, N.; Shafi, M.; Babeker, H.; Lu, J.; et al. The fracture toughness and tribological performance of NiAl/Al_2O_3-40 Wt.% TiO_2 coating generated by air plasma spraying. *Ceram. Int.* **2024**, *50*, 1533–1546. [CrossRef]
17. Wang, C.; Liu, M.; Wang, H.; Jin, G.; Ma, G.; Zhang, J.; Chen, S. Tribological properties and solid particle erosion wear behavior of Al2O3-13 wt%TiO_2/Al_2O_3-PF composite coatings prepared on resin matrix by supersonic plasma spraying. *Ceram. Int.* **2024**, *50*, 29987–29996. [CrossRef]
18. Chang, C.S.T.; Wyss, M.; Andrzejewski, M.; Darut, G.; Graf, L.; Novak, V.; Olbinado, M.; Erpel, S.; Vogel, A.; Bode, S.; et al. Microstructures, phase and mechanical characterisation of Al_2O_3-ZrO_2-TiO_2 coating produced by atmospheric plasma spraying. *Open Ceram.* **2024**, *20*, 100698. [CrossRef]
19. Lv, Y.; Sun, Y.; Deng, C.; Fan, X.; Li, S.; Wang, C.; Yang, Y.; Zhang, Y.; He, C. Preparation, corrosion and tribological properties evolution of self-lubricating Al_2O_3-TiO_2 coatings with superior anti-corrosion. *Surf. Coat. Technol.* **2025**, *498*, 131849. [CrossRef]
20. Girisha, K.; Sreenivas Rao, K.V.; Durga Prasad, C. Slurry Erosion Resistance of Martenistic Stainless Steel with Plasma Sprayed Al_2O_3-40%TiO_2 Coatings. *Mater. Today Proc.* **2018**, *5*, 7388–7393. [CrossRef]
21. Sharma, V.; Kazi, S. Oxidation behaviour of D-gun sprayed Al_2O_3-3 wt% SiC coating. *Surf. Coat. Technol.* **2020**, *383*, 125238. [CrossRef]

22. Łatka, L.; Michalak, M.; Jonda, E. Atmospheric Plasma Spraying of Al_2O_3 + 13% TiO_2 Coatings Using External and Internal Injection System. *Adv. Mater. Sci.* **2019**, *19*, 5–17. [CrossRef]
23. Lu, X.; Yan, D.; Yang, Y.; Dong, Y.; He, J.; Zhang, J. Phase evolution of plasma sprayed $Al_2O_3-13\%TiO_2$ coatings derived from nanocrystalline powders. *Trans. Nonferrous Met. Soc. China* **2013**, *23*, 2951–2956. [CrossRef]
24. Wang, D.S.; Qu, G.; Su, J.L. Thermal Barrier Effects Comparison of Plasma-Sprayed and Laser-Remelted Al_2O_3-13% TiO_2 Ceramic Coatings. *Adv. Mater. Res.* **2014**, *978*, 40–43. [CrossRef]
25. Nguyen Van, T.; Nguyen, T.A.; Pham Thi, H.; Pham Thi, L.; Nguyen Thi, P.; Le Thu, Q. Effect of heat treatment on corrosion resistance of Al_2O_3-TiO_2 ceramic coating impregnated with aluminum phosphate. *Vietnam J. Sci. Technol.* **2024**, *62*, 463–474. [CrossRef]
26. Yu, B.; Zhou, P.; Fang, H.; Wang, Y.; Pu, J. Effects of the TiO_2 content on the mechanical properties and galvanic corrosion resistance of Al_2O_3 coatings. *Ceram. Int.* **2023**, *49*, 38593–38601. [CrossRef]
27. Kawase, M.; Ido, A.; Morinaga, M. Development of $SiO_2/TiO_2/Al_2O_3$-based/TiO_2 coating for preventing sulfide corrosion in thermal power plant boilers. *Appl. Therm. Eng.* **2019**, *153*, 242–249. [CrossRef]
28. Wang, Y.; Tian, W.; Zhang, T.; Yang, Y. Microstructure, spallation and corrosion of plasma sprayed Al_2O_3–13%TiO_2 coatings. *Corros. Sci.* **2009**, *51*, 2924–2931. [CrossRef]
29. Celik, E.; Ozdemir, I.; Avci, E.; Tsunekawa, Y. Corrosion behaviour of plasma sprayed coatings. *Surf. Coat. Technol.* **2005**, *193*, 297–302. [CrossRef]
30. Šuopys, A.; Marcinauskas, L.; Grigaitienė, V.; Kėželis, R.; Aikas, M.; Uscila, R.; Tučkutė, S.; Lelis, M. The Effect of Heat Treatment on the Microstructure and Phase Composition of Plasma Sprayed Al_2O_3 and Al_2O_3-TiO_2 Coatings for Applications in Biomass Firing Plants. *Coatings* **2021**, *11*, 1289. [CrossRef]
31. Šuopys, A.; Grigaitienė, V.; Marcinauskas, L.; Kėželis, R.; Uscila, R.; Aikas, M. Influence of Plasma Torch Power on the Plasma Jet Properties and Microstructure of Alumina Coatings. *Coatings* **2022**, *12*, 934. [CrossRef]
32. Mahade, S.; Mulone, A.; Björklund, S.; Klement, U.; Joshi, S. Incorporation of graphene nano platelets in suspension plasma sprayed alumina coatings for improved tribological properties. *Appl. Surf. Sci.* **2021**, *570*, 151227. [CrossRef]
33. Marcinauskas, L.; Mathew, J.S.; Milieška, M.; Aikas, M.; Kalin, M. Influence of graphite content on the tribological properties of plasma sprayed alumina-graphite coatings. *Surf. Interfaces* **2023**, *38*, 102763. [CrossRef]
34. Song, E.P.; Ahn, J.; Lee, S.; Kim, N.J. Effects of critical plasma spray parameter and spray distance on wear resistance of Al_2O_3–8 wt.%TiO_2 coatings plasma-sprayed with nanopowders. *Surf. Coat. Technol.* **2008**, *202*, 3625–3632. [CrossRef]
35. Ibrahim, K.M.; Havaldar, S.S.; Hiriyannaiah, A.; Keshavamurthy, R. Investigation of Corrosion Characteristics of Plasma-Sprayed Composite Coating on Bearing Steel Through Electrochemical and Salt Spray Test. *J. Bio-Tribo-Corros.* **2022**, *8*, 106. [CrossRef]
36. Wang, Z.; Zhang, J.; Zhang, H.; Li, M.; Li, T.; Wang, Z. Fabrication and Corrosion Resistance of Plasma-Sprayed Glass-Powder-Doped Al_2O_3-13 wt.%TiO_2 Coatings. *J. Therm. Spray Technol.* **2020**, *29*, 500–509. [CrossRef]
37. Bayram, T.; Karabas, M.; Kayali, Y. Deposition and study of plasma sprayed Al_2O_3-TiO_2 coatings on AZ31 magnesium alloy. *Eur. Mech. Sci.* **2023**, *7*, 35–40. [CrossRef]
38. Hakimizad, A.; Raeissi, K.; Golozar, M.A.; Lu, X.; Blawert, C.; Zheludkevich, M.L. The effect of pulse waveforms on surface morphology, composition and corrosion behavior of Al_2O_3 and Al_2O_3 /TiO_2 nano-composite PEO coatings on 7075 aluminum alloy. *Surf. Coat. Technol.* **2017**, *324*, 208–221. [CrossRef]